Optical Fiber Magnetic Field Sensor Based on a Peanut-Shaped Structure Cascaded an FBG

Xueyi Jin[1,a], Lin Huang[2,b], Dongshi Wang[1,c], Haili Yang[2,d], Minyuan Xian[1,e] and Dexing Yang[2,f,*]

[1]Drilling R&D Institute China Oilfield Services Limited Sanhe Hebei, China
[2]MOE Laboratory of Material Physics and Chemistry under Extraordinary Conditions, and Shaanxi Key Laboratory of Optical Information Technology, School of Physical Science and Technology Northwestern Polytechnical University Xi'an, China
a. jinxy5@cosl.com.cn, b. huangllinycxm@163.com, c. wangdsh4@cosl.com.cn, d. 1101092748@qq.com, e. xianmy@cosl.com.cn, f. dxyang@nwpu.edu.cn
**corresponding author: Dexing Yang*

Keywords: Optical fiber magnetic field sensor, peanut-shaped structure, FBG, ferro fluid; cladding mode.

Abstract: A simple and cost-effective optical fiber sensor for magnetic field measurement is represented and demonstrated. The sensor consists of a fiber Bragg grating (FBG) and a peanut-shaped structure cascaded upstream, with ferro fluid coated. The cladding mode can be exited and recoupled to fiber core in the proposed scheme, which benefit the detection of change of refraction index (RI) of ferro fluid induced by the magnetic field exerted. Experiment result shows that the integral intensity of cladding mode in the spectra decreases following with the magnetic field strength increase but increasing with temperature. Moreover, FBG resonance is temperature sensitive, making it possible to detect temperature simultaneously, which can be used to compensate the impact of temperature on magnetic field sensing.

1. Introduction

Ferro fluid, or named magnetic fluid, is usually a very stable colloidal suspension material made of suitable surfactant, liquid carrier, and magnetic nanoparticles evenly dispersed[1]. As a nano-functional material, ferro fluid has got a lot of attention due to its various magneto-optical properties[2], such as Faraday magneto-optic effect, tunable refractive index (RI), field dependent birefringence, and dichroism[3]. Since the magnetic particles are nano-scale, ferro fluids are superparamagnetic and almost show no hysteresis[4,5]. Recently, a variety of optical fiber magnetic field sensors using ferro fluids have been widely studied[6-9]. Most are prepared by coating ferro fluid on the surface of the optical fiber sensing structures, like MZI interferometers and long period fiber gratings[10-12]. These optical fiber sensors for magnetic field measurement is usually

demodulated by the mechanism of RI change of ferro fluid with magnetic field. To improve the sensitivity, these sensors often need some special design for cladding mode excitation in the single mode fiber (SMF).

Cladding mode in fiber is very sensitive to the surrounding RI change because of the evanescent field between the cladding layer and the outer medium. The cladding mode based optical fiber sensor for RI measurement has been extensively investigated for years, in which MZI interferometers could be the most common schemes since they are generally fabricated by fusion splicing fibers with different core diameters to produce cladding mode transmitted in the cladding layer due to the mismatch of modes[13-17]. However, MZI interferometer-based RI sensor is usually wavelength demodulated, which can be limited by the wavelength resolution of the optical spectrum analyzer (OSA). Moreover, these configurations complex the sensing structure or weaken mechanical strength of fiber.

Commonly, FBG-based sensor for temperature and strain measurement is used directly with its core mode reflected resonance varied with Bragg period. While FBG-based RI sensor is usually needed to excite the cladding mode with some special fabrication with FBG, such as misaligned fusion splicing[18], SMF-MMF-SMF configuration[19], spherical structures[20,21], or even directly etching FBG[21-24]. Recently, the cladding mode-based FBG RI sensors have attracted much attention owing to their simplicity and sturdiness, for example, for measurement of bending[21, 25, 26], and more importantly due to its temperature measurement discriminately and simultaneously.

In this letter, a simple and low-cost sensing structure based on an FBG and a peanut fiber structure spliced upstream is proposed, and then coated with ferro fluid as the sensing head for magnetic field measurement with temperature compensation. The proposed sensor scheme is compact, and avoids degrading the fiber strength since no etching and tapering occurs.

2. Operation Principle

The fiber-optical sensing head consists of an FBG and a peanut-shaped structure made by two sphere-like micro-structures fusion-spliced upstream, coated with ferro fluid, as shown in Fig. 1. The peanut-shaped structure can couple core mode to cladding mode thus exciting the cladding mode due to the diameter of fiber core variations. When propagating at the FBG section, part of the forward transmitted cladding mode will recouple to core mode, and then transmit backward to reach the peanut-shaped structure again. The core mode will reflect by FBG when the phase is matched with the resonance wavelength of Bragg wavelength. Therefore, the whole reflection spectrum of the sensing head includes both the core mode and the cladding mode.

The reflected spectrum of the proposed scheme exhibits different response to the applied magnetic field strength and environmental temperature, respectively. The intensity of the reflection spectra of cladding mode is sensitive to external RI change due to strong evanescent field resulting from the mode field mismatch of the peanut-shaped structure. After coated by ferro fluid, the cladding mode amplitude will vary directly with the absorption, as well as scattering of ferro fluid. Since magnetic field and temperature changes can influence the RI of ferro fluid, the cladding mode amplitude, or the reflection spectra intensity will be magnetic field and temperature dependent. Besides, FBG is highly temperature sensitive, enabling the measurement of magnetic field strength with temperature compensation.

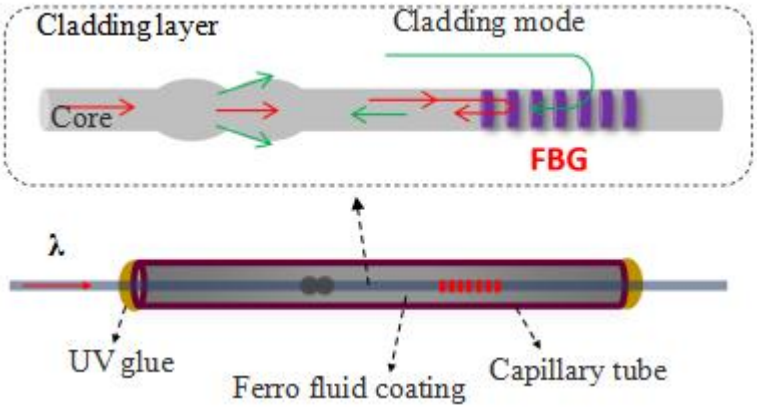

Figure 1: Schematic diagram of the sensing structure.

Figure 1 shows the sensing mechanism of the proposed sensor. As light is launched to the peanut-shaped fiber structure from the leading SMF, multiple cladding modes can be excited due to mode field mismatch. When forward propagating to the downstream FBG, both core mode and cladding mode are reflected[27,28], and then the backward reflected lights can reach the peanut-shaped structure again soon. As light propagates back through the peanut-shaped structure, another series of cladding modes are excited by core mode which are attenuated in the cladding layer because of the evanescent field. In the meantime, the reflected cladding mode by FBG will be recoupled to the core mode at the peanut-shaped structure section. Since the cladding mode is sensitive to the SRI, the counter-propagated spectra can respond to the RI changed of the ferro fluid. As a result, the magnetic field can be demodulated by monitoring the cladding mode spectra.

According to the diffraction theory, light propagating at FBG should satisfy the Bragg Equation:

$$n\sin\theta_1 - n\sin\theta_2 = \frac{\lambda}{\Lambda} \tag{1}$$

where n denotes the RI of the cladding layer, and λ denotes the resonance wavelength, Λ represents the FBG period, θ_1 and θ_2 denote the incident and reflected angle respectively when light diffracted at FBG.

For the i^{th} cladding mode, $\theta_{1i} = -\theta_{2i}$,

$$\lambda_i = 2n_{cl,i}\Lambda \tag{2}$$

where $n_{cl,i}=n\sin\theta$, is the effective index of the its cladding mode when diffracting at FBG.

Since the peanut-shaped structure is upstream the FBG, the incident angle of cladding mode will be less than that of the fundamental core mode. That is,

$$\lambda_i < \lambda_{FBG} \tag{3}$$

Therefore, the resonance peaks of cladding modes are all at short-wavelength side of the Bragg resonance peak (λ_{FBG}). When propagating along the fiber, the incident angles cell, incident of the cladding modes at the interface of the cladding and the surrounding medium will be smaller than that of the core mode at the interface of the core and the cladding, and they satisfy the total internal

reflection. For a high-order cladding mode, the evanescent field penetration depth will increase as the incident angle get close to the critical angle, which can be derived from

$$d_z = \frac{\lambda}{2\pi\sqrt{\sin^2\theta_{cl,incident} - \left(\frac{n_{medium}}{n_{cl}}\right)^2}} \tag{4}$$

where d_z denotes the evanescent field penetration depth, and mediums is the refractive index of surrounding medium, of which the imaginary part will cause absorption. Thus, the light intensity of the high-order cladding modes will be more strongly absorbed than the relatively low-order ones. The short wavelength resonance peaks of the reflection spectra are resulting from the coupling of high–order cladding mode and the core mode, with great penetration depth. Consequently, their intensity will attenuate more sharply because of the absorption of ferro fluid. Since the amplitude of high-order modes are usually small, the dynamic range of the peaks with shorter wavelength will be restricted. That is, the peaks with intermediate wavelength of the reflection spectra could be the subject of study.

3. Sensor Design

The core and cladding diameter of the used SMF are 8.3μm and 125μm respectively. The peanut-shaped structure is fabricated by splicing the FBG and a SMF through a commercial fusion splicer. The center wavelength of FBG resonance is 1534.49nm under room temperature with a reflectivity of 98%. To prepare the peanut-shaped fiber structure, a spherical fiber structure is fabricated at the end of SMF previously by discharging in the fusion splicer. Then two spherical structures are fusion-spliced together to form the peanut-shaped fiber structure. The distance between the peanut-shaped structure and FBG is set to 1cm to avoid damaging FBG while discharging. The distance between the two spherical structures and the diameter of the joint waist of the formed peanut-shaped structure are 167.78μm and 101.89μm, respectively, as shown in Figure 2.

The entire structure consisting of the peanut-shaped structure and FBG is threaded through a capillary glass tube with ferro fluid filled subsequently, and later is sealed by UV glue, forming the sensing head. To get rid of undesirable reflection, the end face of fiber pigtail is kept rough and better japanning. During the packaging process, the air bubble is needed to be removed completely from ferro fluid to eliminate the impact on the RI from it.

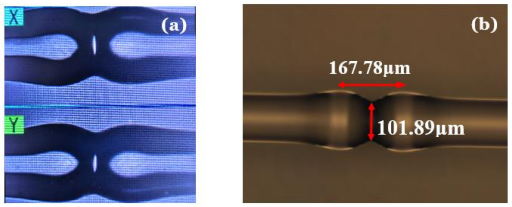

Figure 2: The image of the peanut-shaped structure (a) in fusion splicer, (b) under microscope.

The experimental setup for performing the magnetic field and temperature sensing is shown in Figure 3, including an Amplified Spontaneous Emission (ASE) and an Optical Spectra Analyzer (OSA). The magnetic field is generated and adjusted by regulating the current of an electromagnets pair, and is set perpendicular to the fiber probe. A magnetic Gauss meter is employed to measure the applied magnetic field strength. Light is launched from the ASE into the sensor probe via a circulator,

and the reflected light will go back through the circulator later again to OSA. The temperature is controlled by climate chamber.

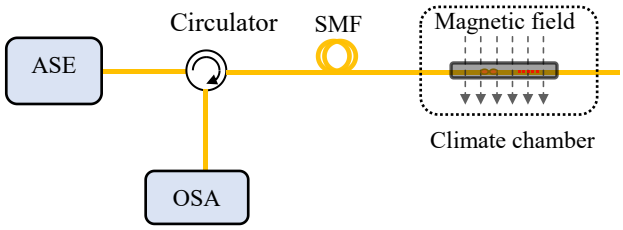

Figure 3: Schematic diagram of the experiment setup for magnetic field and temperature sensing.

4. Results and Discussion

At room temperature, the magnetic nano-particles in the ferro fluid will gather to form chains and even columns when applied magnetic field, leading to solid-liquid separation and the consequent change of RI[29]. As a result, the cladding mode intensity in the reflection spectra decreases due to the evanescent field as Figure 4 shows.

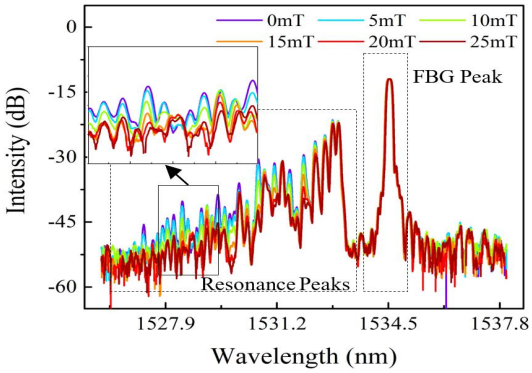

Figure 4: Reflection spectra of the sensor under different magnetic field strength at 25℃.

In the reflected spectra, different order cladding mode can be observed and its intensity decreases following with the magnetic field increase as Figure 4 shows. However, the cladding mode resonance peaks decreases with differently amount. In the lower magnetic field range of 0−15mT, a single resonance peak at 1528.95nm has the most amount of intensity decrease, but soon leveling off when filed is larger, as Figure 5 shows. While in the higher magnetic field range from 15−25mT, another single resonance peak at 1529.71nm has the highest wavelength shift rate, but slowing in the lower magnetic field range. Moreover, these two indicators respond linearly to the corresponding magnetic field range with sensitivity of −0.60dB/MT and 6.55pm/mT respectively, and each can be responsible for a single sensing range.

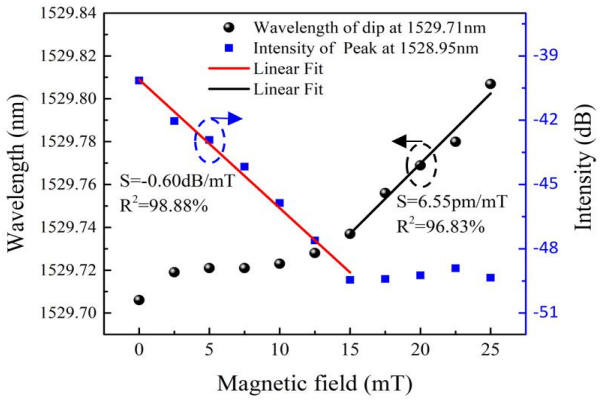

Figure 5: Magnetic field sensing at 25°C using two indicators together to obtain a wide sensing range.

Therefore, a wide-range linear magnetic field sensing covering the saturation and the starting end can be realized at room temperature by combining the above two indicators, which could be concluded as

$$\begin{cases} \Delta I_{peak} = -0.6\Delta B \\ \Delta \lambda_{dip} = 6.55\Delta B \end{cases} \tag{5}$$

where ΔI_{peak} and $\Delta \lambda_{dip}$ denote the intensity variation of the detected peak at 1528.95nm, and the wavelength shift of the chosen dip initially at 1529.71nm in the reflected reflection spectra.During the process, the center wavelength and the intensity of the Bragg peak remain nearly steady, as Figure 6 shows.

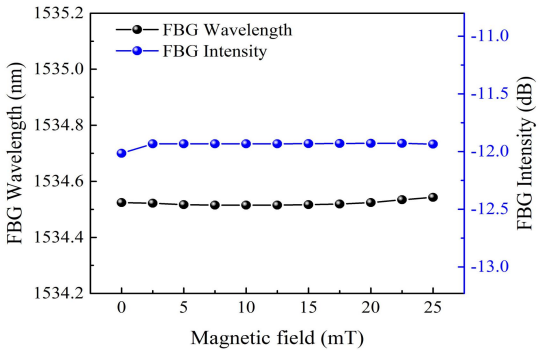

Figure 6: The center wavelength and the intensity of the Bragg peak response to different magnetic field strength at room temperature.

To test the influence by different temperature, the reflected spectra of the sensor is investigated at a certain magnetic field strength. Unfortunately, the intensity of cladding mode changes complexly with some decreased while others increased when temperature increases.

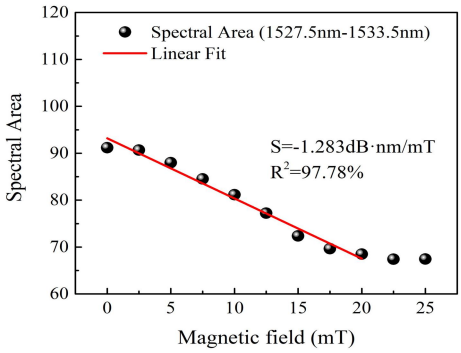

Figure 7: The integral relative intensity of reflection spectra response to different magnetic field strength.

To be simple, the integral intensity of the reflection spectra from 1527.5nm to 1533.5nm is chosen as the sensing indicator since it decreases linearly with sensitivity of −1.283dB·nm/mT to magnetic field from 0 up to 20mT, as is shown in Figure 7.

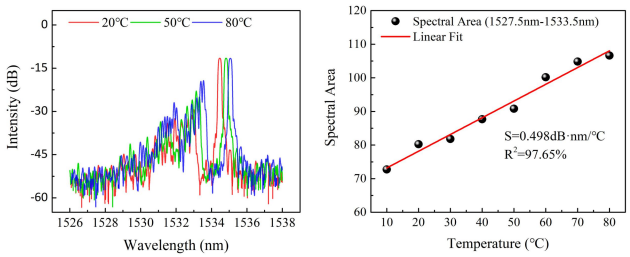

Figure 8: (a) The wavelength response of reflection spectra, and (b) the integral relative intensity of reflection spectra response to different temperature.

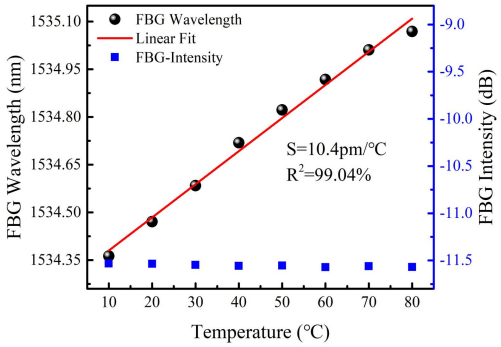

Figure 9: The measured Bragg wavelength shifts with the temperature.

As mentioned above, the integral intensity ($I_{integral}$) of the reflection spectra is also temperature dependent. Figure 8 (a) shows the reflection spectra overall red-shifts with temperature rising from 10℃ up to 80℃, and Figure 8 (b) gives that the integral intensity of reflection spectra from 1527.5nm to 1533.5nm responds almost linearly to different temperature with sensitivity of 0.498dB·nm/℃.

Due to the Bragg wavelength red-shift proportional to temperature, the ambient temperature can be measured independently with sensitivity of 10.4pm/℃, as Figure 9 shows. Thus, the sensing of

the magnetic field strength can be acquired with temperature compensation by the following equations

$$\begin{bmatrix} \Delta\lambda_{\text{FBG}} \\ \Delta I_{\text{integral}} \end{bmatrix} = \begin{bmatrix} 0.0104 & 0 \\ 0.498 & -1.283 \end{bmatrix} \begin{bmatrix} \Delta T \\ \Delta B \end{bmatrix} \tag{6}$$

Acknowledgments

This work is supported by the National Science and Technology Major Project of China under Grant (2016ZX05028-001).

References

[1] Odenbach, S., 'Recent Progress in Magnetic Fluid Research', Journal of Physics: Condensed Matter, 2004, 16, (32), pp. R1135-R1150.

[2] Davies, H.W. and Llewellyn, J.P., 'Magneto-Optic Effects in Ferrofluids', Journal of Physics D Applied Physics, 2000, 13, (12), pp. 2327-2336.

[3] Du, B., Yang, D., Bai, Y., Yuan, Y., Mao, D., Zhang, W., and She, X., 'Investigation of Magneto-Induced Linear Dichroism of Magnetic Fluid', Applied Optics, 2017, 56, (3), pp. 739-742.

[4] Wu, S., Sun, A. , Zhai, F. , Wang, J. , Xu, W. , & Zhang, Q, 'Fe3o4 Magnetic Nanoparticles Synthesis from Tailings by Ultrasonic Chemical Co-Precipitation ', Materials Letters, 2011, 65, (12), pp. 1882-1884.

[5] del Barco, E., Asenjo, J., Zhang, X.X., Pieczynski, R., Julià, A., Tejada, J., Ziolo, R.F., Fiorani, D., and Testa, A.M., 'Free Rotation of Magnetic Nanoparticles in a Solid Matrix', Chemistry of Materials, 2001, 13, (5), pp. 1487-1490.

[6] Peng, Z., Chi Chiu, C., Siang, L.W., Yongxing, J., Yifan, Z., Hwi Fen, L., Li Han, C., Chang, W.W., and Xinyong, D., 'Magneto-Optical Fiber Sensor Based on Magnetic Fluid', OPTICS LETTERS, 2012, 37, (3), pp. 398-400.

[7] Luo, L., Pu, S., Tang, J., Zeng, X., and Lahoubi, M., 'Reflective All-Fiber Magnetic Field Sensor Based on Microfiber and Magnetic Fluid', Optics Express, 2015, 23, (14), pp. 18133-18142.

[8] Ying, Y., Zhang, R., Si, G.-Y., Wang, X., and Qi, Y.-W., 'D-Shaped Tilted Fiber Bragg Grating Using Magnetic Fluid for Magnetic Field Sensor', Optics Communications, 2017, 405, (1), pp. 228-232.

[9] Tian, Q., Feng, Z., Rong, Q., Wan, Y., Qiao, X., Hu, M., Yang, H., Wang, R., Shao, Z., and Yang, T., 'A Temperature-Independent Fibre-Optic Magnetic-Field Sensor Using Thin-Core Fibre Tailored Fibre Bragg Grating', Optics Communications, 2017, 393, (1), pp. 169-172.

[10] Jie, Z., Xinyong, D., Peng, Z., Li-Yang, S., Chi Chiu, C., Ying, C., and Perry Ping, S., 'Magnetic Field Sensor Using Tilted Fiber Grating Interacting with Magnetic Fluid', Optics Express, 2013, 21, (15), pp. 17863-17868.

[11] Zhao, Y., Lv, R.-q., Ying, Y., and Wang, Q., 'Hollow-Core Photonic Crystal Fiber Fabry–Perot Sensor for Magnetic Field Measurement Based on Magnetic Fluid', Optics & Laser Technology, 2012, 44, (4), pp. 899-902.

[12] Gao, L., Zhu, T., Deng, M., Chiang, K.S., Sun, X., Dong, X., and Hou, Y., 'Long-Period Fiber Grating within D-Shaped Fiber Using Magnetic Fluid for Magnetic-Field Detection', IEEE Photonics Journal, 2012, 4, (6), pp. 2095-2104.

[13] Zi, D.X., Hang-Zhou, Y., Xue-Guang, Q., Pan, Z., Oin, T., Zhou, R.Q., Mohd, N.N.A., Kok-Sing, L., and Harith, A., 'Mach–Zehnder Interferometric Magnetic Field Sensor Based on a Photonic Crystal Fiber and Magnetic Fluid', Applied Optics, 57, (9), pp. 2050-.

[14] Chen, Y. and Wu, X., 'Optical Fiber Magnetic Sensor Based on Magnetic Fluid and Long Period Fiber Grating', in, 17th International Conference on Optical Communications and Networks (ICOCN2018), (International Society for Optics and Photonics, 2019)

[15] Sun, B., Fang, F., Zhang, Z., Xu, J., and Zhang, L., 'High-Sensitivity and Low-Temperature Magnetic Field Sensor Based on Tapered Two-Mode Fiber Interference', OPTICS LETTERS, 2018, 43, (6), pp. 1311-1314.

[16] Dong, Y., Wu, B., Wang, M., Xiao, H., Xiao, S., Sun, C., Li, H., and Jian, S., 'Magnetic Field and Temperature Sensor Based on D-Shaped Fiber Modal Interferometer and Magnetic Fluid', Optics & Laser Technology, 2018, 107, pp. 169-173.

[17] Li, X.-g., Zhou, X., Zhao, Y., and Lv, R.-Q., 'Multi-Modes Interferometer for Magnetic Field and Temperature Measurement Using Photonic Crystal Fiber Filled with Magnetic Fluid', Optical Fiber Technology, 2018, 41, pp. 1-6.

[18] Gouveia, C., Jorge, P., Baptista, J., and Frazao, O., 'Temperature-Independent Curvature Sensor Using Fbg Cladding Modes Based on a Core Misaligned Splice', IEEE Photonics Technology Letters, 2011, 23, (12), pp. 804-806.

[19] Zaini, M.K.A.B., Lee, Y., Lim, K., Ali, M.M., Nazal, N.A.M., and Ahmad, H., 'Digital Matched Filtering (Dmf) Technique for the Performance Enhancement of Few-Mode Fiber Bragg Grating Sensor', IEEE Sensors Journal, 2019, 19, (14), pp. 5653-5659.

[20] Gu, M., Yuan, S., Yuan, Q., and Tong, Z., 'Temperature-Independent Refractive Index Sensor Based on Fiber Bragg Grating and Spherical-Shape Structure', Optics and Lasers in Engineering, 2019, 115, pp. 86-89.

[21] Wang, Z., Shi-Li, L., Sun, M., and Jin, Y., 'Temperature-Insensitive Curvature Sensor Based on a Peanut-Shape Structure and a Fbg', Acta Photonica Sinica, 2016, 45, p. 1106006.

[22] Luo, D., Ma, J., Ibrahim, Z., and Ismail, Z., 'Etched Fbg Coated with Polyimide for Simultaneous Detection the Salinity and Temperature', Optics Communications, 2017, 392, pp. 218-222.

[23] Ray, P., Srijith, K., and Srinivasan, B., 'Enhanced Sensitivity Etched Fiber Bragg Gratings for Precise Measurement of Refractive Index', in, International Conference on Optics and Photonics 2015, (International Society for Optics and Photonics, 2015)

[24] Fu, H., Zhang, J., Ding, J., Wang, Q., Li, H., Shao, M., Liu, Y., Liu, Q., Zhang, M., and Zhu, Y., 'Ultra Sensitive Nh3 Gas Detection Using Microfiber Bragg Grating', Optics Communications, 2018, 427, pp. 331-334.

[25] Sun, A. and Wu, Z., 'Temperature Insensitive Bending Sensor Based on Microbending Fbg Cladding Mode Recoupling', Microwave and Optical Technology Letters, 2012, 54, (7), pp. 1674-1676.

[26] Su, D., Qiao, X., Chen, F., and Rong, Q., 'Higher Order Coupling Mode for Orientation-Dependent Bend Measurement Using an Off-Axis Fbg Inscription over Few-Mode Fiber', IEEE Sensors Journal, 2019, 19, (4), pp. 1368-1372.

[27] Sáez-Rodriguez, D., Cruz, J.L., Díez, A., and Andrés, M.V., 'Coupling between Counterpropagating Cladding Modes in Fiber Bragg Gratings', OPTICS LETTERS, 2011, 36, (8), pp. 1518-1520.

[28] Zhang, A.-P., Tao, X.-M., Chung, W.-H., Guan, B.-O., and Tam, H.-Y., 'Cladding-Mode-Assisted Recouplings in Concatenated Long-Period and Fiber Bragg Gratings', OPTICS LETTERS, 2002, 27, (14), pp. 1214-1216.

[29] Yang, D., Du, L., Xu, Z., Jiang, Y., Xu, J., Wang, M., Bai, Y., and Wang, H., 'Magnetic Field Sensing Based on Tilted Fiber Bragg Grating Coated with Nanoparticle Magnetic Fluid', Applied Physics Letters, 2014, 104, (6), p. 061903.pan, p. 301, 1982].

[30] M. Young, The Technical Writer's Handbook. Mill Valley, CA: University Science, 1989.ing published.